EUROPEAN LABORATORY FOR PARTICLE PHYSICS

CERN/PPE/97-10
January 22, 1997

Study of muon-pair production at centre-of-mass energies from 20 to 136 GeV with the ALEPH detector

The ALEPH Collaboration

Abstract

The total cross section and the forward-backward asymmetry for the process $e^+e^- \to \mu^+\mu^-(n\gamma)$ are measured in the energy range 20-136 GeV by reconstructing the effective centre-of-mass energy after initial state radiation. The analysis is based on the data recorded with the ALEPH detector at LEP between 1990 and 1995, corresponding to a total integrated luminosity of 143.5 pb^{-1}. Two different approaches are used: in the first one an exclusive selection of events with hard initial state radiation in the energy range 20-88 GeV is directly compared with the Standard Model predictions showing good agreement. In the second one, all events are used to obtain a precise measurement of the energy dependence of σ^0 and $A^0_{\rm FB}$ from a model independent fit, enabling constraints to be placed on models with extra Z bosons.

(submitted to Physics Letters B)

R. Barate, D. Buskulic, D. Decamp, P. Ghez, C. Goy, J.-P. Lees, A. Lucotte, M.-N. Minard, J.-Y. Nief, P. Odier, B. Pietrzyk

Laboratoire de Physique des Particules (LAPP), IN^{2}P^3-CNRS, 74019 Annecy-le-Vieux Cedex, France

M.P. Casado, M. Chmeissani, P. Comas, J.M. Crespo, M. Delfino, E. Fernandez, M. Fernandez-Bosman, Ll. Garrido,[15] A. Juste, M. Martinez, S. Orteu, C. Padilla, I.C. Park, A. Pascual, J.A. Perlas, I. Riu, F. Sanchez, F. Teubert

Institut de Fisica d'Altes Energies, Universitat Autonoma de Barcelona, 08193 Bellaterra (Barcelona), Spain[7]

A. Colaleo, D. Creanza, M. de Palma, G. Gelao, G. Iaselli, G. Maggi, M. Maggi, N. Marinelli, S. Nuzzo, A. Ranieri, G. Raso, F. Ruggieri, G. Selvaggi, L. Silvestris, P. Tempesta, A. Tricomi,[3] G. Zito

Dipartimento di Fisica, INFN Sezione di Bari, 70126 Bari, Italy

X. Huang, J. Lin, Q. Ouyang, T. Wang, Y. Xie, R. Xu, S. Xue, J. Zhang, L. Zhang, W. Zhao

Institute of High-Energy Physics, Academia Sinica, Beijing, The People's Republic of China[8]

D. Abbaneo, R. Alemany, A.O. Bazarko, P. Bright-Thomas, M. Cattaneo, F. Cerutti, H. Drevermann, R.W. Forty, M. Frank, R. Hagelberg, J. Harvey, P. Janot, B. Jost, E. Kneringer, J. Knobloch, I. Lehraus, G. Lutters, P. Mato, A. Minten, R. Miquel, Ll.M. Mir,[2] L. Moneta, T. Oest,[1] A. Pacheco, J.-F. Pusztaszeri, F. Ranjard, P. Rensing,[25] G. Rizzo, L. Rolandi, D. Schlatter, M. Schmelling,[24] M. Schmitt, O. Schneider, W. Tejessy, I.R. Tomalin, A. Venturi, H. Wachsmuth, A. Wagner

European Laboratory for Particle Physics (CERN), 1211 Geneva 23, Switzerland

Z. Ajaltouni, A. Barrès, C. Boyer, A. Falvard, C. Ferdi, P. Gay, C. Guicheney, P. Henrard, J. Jousset, B. Michel, S. Monteil, J-C. Montret, D. Pallin, P. Perret, F. Podlyski, J. Proriol, P. Rosnet, J.-M. Rossignol

Laboratoire de Physique Corpusculaire, Université Blaise Pascal, IN^{2}P^3-CNRS, Clermont-Ferrand, 63177 Aubière, France

T. Fearnley, J.B. Hansen, J.D. Hansen, J.R. Hansen, P.H. Hansen, B.S. Nilsson, B. Rensch, A. Wäänänen

Niels Bohr Institute, 2100 Copenhagen, Denmark[9]

G. Daskalakis, A. Kyriakis, C. Markou, E. Simopoulou, A. Vayaki, K. Zachariadou

Nuclear Research Center Demokritos (NRCD), Athens, Greece

A. Blondel, J.C. Brient, F. Machefert, A. Rougé, M. Rumpf, A. Valassi,[6] H. Videau

Laboratoire de Physique Nucléaire et des Hautes Energies, Ecole Polytechnique, IN^{2}P^3-CNRS, 91128 Palaiseau Cedex, France

E. Focardi,[21] G. Parrini

Dipartimento di Fisica, Università di Firenze, INFN Sezione di Firenze, 50125 Firenze, Italy

M. Corden, C. Georgiopoulos, D.E. Jaffe

Supercomputer Computations Research Institute, Florida State University, Tallahassee, FL 32306-4052, USA [13,14]

A. Antonelli, G. Bencivenni, G. Bologna,[4] F. Bossi, P. Campana, G. Capon, D. Casper, V. Chiarella, G. Felici, P. Laurelli, G. Mannocchi,[5] F. Murtas, G.P. Murtas, L. Passalacqua, M. Pepe-Altarelli

Laboratori Nazionali dell'INFN (LNF-INFN), 00044 Frascati, Italy

L. Curtis, S.J. Dorris, A.W. Halley, I.G. Knowles, J.G. Lynch, V. O'Shea, C. Raine, J.M. Scarr, K. Smith, P. Teixeira-Dias, A.S. Thompson, E. Thomson, F. Thomson, R.M. Turnbull

Department of Physics and Astronomy, University of Glasgow, Glasgow G12 8QQ,United Kingdom[10]

J. Sommer, H. Stenzel, K. Tittel, S. Werner, M. Wunsch

Institut für Hochenergiephysik, Universität Heidelberg, 69120 Heidelberg, Fed. Rep. of Germany[16]

R. Beuselinck, D.M. Binnie, W. Cameron, P.J. Dornan, M. Girone, S. Goodsir, E.B. Martin, P. Morawitz, A. Moutoussi, J. Nash, J.K. Sedgbeer, A.M. Stacey, M.D. Williams

Department of Physics, Imperial College, London SW7 2BZ, United Kingdom[10]

G. Dissertori, P. Girtler, D. Kuhn, G. Rudolph

Institut für Experimentalphysik, Universität Innsbruck, 6020 Innsbruck, Austria[18]

A.P. Betteridge, C.K. Bowdery, P. Colrain, G. Crawford, A.J. Finch, F. Foster, G. Hughes, R.W. Jones, T. Sloan, E.P. Whelan, M.I. Williams

Department of Physics, University of Lancaster, Lancaster LA1 4YB, United Kingdom[10]

C. Hoffmann, K. Jakobs, K. Kleinknecht, G. Quast, B. Renk, E. Rohne, H.-G. Sander, P. van Gemmeren, C. Zeitnitz

Institut für Physik, Universität Mainz, 55099 Mainz, Fed. Rep. of Germany[16]

J.J. Aubert, C. Benchouk, A. Bonissent, G. Bujosa, D. Calvet, J. Carr, P. Coyle, C. Diaconu, N. Konstantinidis, O. Leroy, P. Payre, D. Rousseau, M. Talby, A. Sadouki, M. Thulasidas, A. Tilquin, K. Trabelsi

Centre de Physique des Particules, Faculté des Sciences de Luminy, IN^2P^3-CNRS, 13288 Marseille, France

M. Aleppo, F. Ragusa[21]

Dipartimento di Fisica, Università di Milano e INFN Sezione di Milano, 20133 Milano, Italy.

R. Berlich, W. Blum, V. Büscher, H. Dietl, F. Dydak,[21] G. Ganis, C. Gotzhein, H. Kroha, G. Lütjens, G. Lutz, W. Männer, H.-G. Moser, R. Richter, A. Rosado-Schlosser, S. Schael, R. Settles, H. Seywerd, R. St. Denis, H. Stenzel, W. Wiedenmann, G. Wolf

Max-Planck-Institut für Physik, Werner-Heisenberg-Institut, 80805 München, Fed. Rep. of Germany[16]

J. Boucrot, O. Callot,[21] S. Chen, A. Cordier, M. Davier, L. Duflot, J.-F. Grivaz, Ph. Heusse, A. Höcker, A. Jacholkowska, M. Jacquet, D.W. Kim,[19] F. Le Diberder, J. Lefrançois, A.-M. Lutz, I. Nikolic, H.J. Park,[19] M.-H. Schune, S. Simion, J.-J. Veillet, I. Videau, D. Zerwas

Laboratoire de l'Accélérateur Linéaire, Université de Paris-Sud, IN^2P^3-CNRS, 91405 Orsay Cedex, France

P. Azzurri, G. Bagliesi, G. Batignani, S. Bettarini, C. Bozzi, G. Calderini, M. Carpinelli, M.A. Ciocci, V. Ciulli, R. Dell'Orso, R. Fantechi, I. Ferrante, A. Giassi, A. Gregorio, F. Ligabue, A. Lusiani, P.S. Marrocchesi, A. Messineo, F. Palla, G. Sanguinetti, A. Sciabà, P. Spagnolo, J. Steinberger, R. Tenchini, G. Tonelli,[20] C. Vannini, P.G. Verdini

Dipartimento di Fisica dell'Università, INFN Sezione di Pisa, e Scuola Normale Superiore, 56010 Pisa, Italy

G.A. Blair, L.M. Bryant, J.T. Chambers, Y. Gao, M.G. Green, T. Medcalf, P. Perrodo, J.A. Strong, J.H. von Wimmersperg-Toeller

Department of Physics, Royal Holloway & Bedford New College, University of London, Surrey TW20 OEX, United Kingdom[10]

D.R. Botterill, R.W. Clifft, T.R. Edgecock, S. Haywood, P. Maley, P.R. Norton, J.C. Thompson, A.E. Wright

Particle Physics Dept., Rutherford Appleton Laboratory, Chilton, Didcot, Oxon OX11 OQX, United Kingdom[10]

B. Bloch-Devaux, P. Colas, W. Kozanecki, E. Lançon, M.C. Lemaire, E. Locci, P. Perez, J. Rander, J.-F. Renardy, A. Roussarie, J.-P. Schuller, J. Schwindling, A. Trabelsi, B. Vallage

CEA, DAPNIA/Service de Physique des Particules, CE-Saclay, 91191 Gif-sur-Yvette Cedex, France[17]

S.N. Black, J.H. Dann, H.Y. Kim, A.M. Litke, M.A. McNeil, G. Taylor

Institute for Particle Physics, University of California at Santa Cruz, Santa Cruz, CA 95064, USA[22]

C.N. Booth, R. Boswell, C.A.J. Brew, S. Cartwright, F. Combley, M.S. Kelly, M. Letho, W.M. Newton, J. Reeve, L.F. Thompson

Department of Physics, University of Sheffield, Sheffield S3 7RH, United Kingdom[10]

K. Affholderbach, A. Böhrer, S. Brandt, G. Cowan, C. Grupen, P. Saraiva, L. Smolik, F. Stephan

Fachbereich Physik, Universität Siegen, 57068 Siegen, Fed. Rep. of Germany[16]

M. Apollonio, L. Bosisio, R. Della Marina, G. Giannini, B. Gobbo, G. Musolino

Dipartimento di Fisica, Università di Trieste e INFN Sezione di Trieste, 34127 Trieste, Italy

J. Putz, J. Rothberg, S. Wasserbaech, R.W. Williams

Experimental Elementary Particle Physics, University of Washington, WA 98195 Seattle, U.S.A.

S.R. Armstrong, P. Elmer, Z. Feng,[12] D.P.S. Ferguson, Y.S. Gao,[23] S. González, J. Grahl, T.C. Greening, O.J. Hayes, H. Hu, P.A. McNamara III, J.M. Nachtman, W. Orejudos, Y.B. Pan, Y. Saadi, I.J. Scott, J. Walsh, Sau Lan Wu, X. Wu, J.M. Yamartino, M. Zheng, G. Zobernig

Department of Physics, University of Wisconsin, Madison, WI 53706, USA[11]

[1]Now at DESY, Hamburg, Germany.
[2]Supported by Dirección General de Investigación Científica y Técnica, Spain.
[3]Also at Dipartimento di Fisica, INFN Sezione di Catania, Catania, Italy.
[4]Also Istituto di Fisica Generale, Università di Torino, Torino, Italy.
[5]Also Istituto di Cosmo-Geofisica del C.N.R., Torino, Italy.
[6]Supported by the Commission of the European Communities, contract ERBCHBICT941234.
[7]Supported by CICYT, Spain.
[8]Supported by the National Science Foundation of China.
[9]Supported by the Danish Natural Science Research Council.
[10]Supported by the UK Particle Physics and Astronomy Research Council.
[11]Supported by the US Department of Energy, grant DE-FG0295-ER40896.
[12]Now at The Johns Hopkins University, Baltimore, MD 21218, U.S.A.
[13]Supported by the US Department of Energy, contract DE-FG05-92ER40742.
[14]Supported by the US Department of Energy, contract DE-FC05-85ER250000.
[15]Permanent address: Universitat de Barcelona, 08208 Barcelona, Spain.
[16]Supported by the Bundesministerium für Bildung, Wissenschaft, Forschung und Technologie, Fed. Rep. of Germany.
[17]Supported by the Direction des Sciences de la Matière, C.E.A.
[18]Supported by Fonds zur Förderung der wissenschaftlichen Forschung, Austria.
[19]Permanent address: Kangnung National University, Kangnung, Korea.
[20]Also at Istituto di Matematica e Fisica, Università di Sassari, Sassari, Italy.
[21]Also at CERN, 1211 Geneva 23, Switzerland.
[22]Supported by the US Department of Energy, grant DE-FG03-92ER40689.
[23]Now at Harvard University, Cambridge, MA 02138, U.S.A.
[24]Now at Max-Plank-Institüt für Kernphysik, Heidelberg, Germany.
[25]Now at Dragon Systems, Newton, MA 02160, U.S.A.

1 Introduction

The muon pair cross section and forward-backward asymmetry have been accurately measured at different energy points around the Z mass [1]. These measurements allow a precise determination of the effective couplings of the Z to muons. The vector and axial vector couplings of the Z , together with the known photon couplings, completely determine the behaviour of the cross section and forward-backward asymmetry at any energy, if no new physics beyond the Standard Model is present.

In a more general framework, however, the description of the energy dependence of these quantities requires the introduction of new parameters, as done, for example in the S-matrix formalism (ref. [2]), which can be determined from the present measurements at LEP only with limited precision.

Radiative muon events can be used to explore an interval of energies much broader than the nominal LEP energy range, and to improve the knowledge on these parameters.

So far, the analysis of radiative muon events carried out by other experiments [3] has been based on the exclusive selection of events with hard initial state radiation (ISR) photons. This approach has been followed in this paper and the results compare well with the Standard Model (SM) expectations.

In addition, a more general method (inclusive analysis) has been developed in which the effective centre-of-mass energy after ISR is determined on an event-by-event basis. This approach allows the use of all muon events. As a consequence, the sensitivity to the parameters describing the energy dependence of the cross section and forward-backward asymmetry is maximized, allowing as well the LEP constraints on the existence of new Z bosons to be improved.

The outline of this paper is the following: in section 2 the theoretical justification of this new approach is analyzed. In section 3 a brief description of the ALEPH detector with its performances and the Monte Carlo generators used are given. Section 4 is devoted to the discussion of the event selection and the two analysis methods. In section 5 the results and a summary of the main systematic uncertainties are presented. Finally in sections 6 and 7, limits on extra Z bosons and conclusions are given.

2 Theoretical formalism

The probability density that describes the process $e^+e^- \to \mu^+\mu^-(n\gamma)$ at a given centre-of-mass energy $\sqrt{s}$ can be written as

$$\frac{\mathrm{d}^2\hat{\sigma}}{\mathrm{d}x\ \mathrm{d}\cos\theta}(s) \;=\; \frac{1}{\sigma(s)} H(s,x)\left[\frac{3}{8}\sigma^0_{\mathrm{T}}(s')(1+\cos^2\theta) + \sigma^0_{\mathrm{FB}}(s')\cos\theta\right]. \qquad (1)$$

Here θ is the scattering angle of one of the outgoing fermions with respect to the beam of the same sign in the centre-of-mass of the hard process, and $s' \equiv s(1-x)$ is the invariant

mass of the colliding e^+e^- system after ISR. x is the fraction of radiated beam energy if only one photon is emitted in the initial state. All the electroweak radiative corrections, Z and γ vacuum polarization, vertex and box corrections are absorbed in the definition of the total cross section $\sigma^0_{\rm T}$ and the antisymmetric (w.r.t. θ) cross section $\sigma^0_{\rm FB}$, while $H(s,x)$ is the radiator function that accounts for QED bremsstrahlung corrections [4]. The integral of the differential cross section, $\sigma(s)$, is used to normalize the probability density.

One can think of $\sqrt{s'}$ as the "effective" centre-of-mass energy after ISR. This interpretation is only valid if the interference between initial and final state photon radiation (FSR) can be neglected. Moreover, this interference distorts the angular distribution of Eq. (1). The effect of ISR-FSR interference is predicted to be small [5] at $\sqrt{s} \sim M_Z$, if no tight cuts are placed on the photon phase space. This is not, however, true when the variable s' (or x) in Eq. (1) is not integrated. The differential x distribution is thus binned in intervals of size greater than the Z width, $\Delta x = 0.04 > \Gamma_{\rm Z}/M_{\rm Z}$. Such a choice reduces the effect of the overlap between initial and final state wavefunctions and hence diminishes the influence of ISR-FSR interference.

The probability density of Eq. (1) is only positive defined for all values of $\cos\theta$ when $\mid \sigma^0_{\rm FB} \mid < \frac{3}{4}\sigma^0_{\rm T}$. This is not a problem when the measured asymmetry ($A^0_{\rm FB} \equiv \sigma^0_{\rm FB}/\sigma^0_{\rm T}$) is far from this theoretical constraint, but would introduce strong correlations between the fitted parameters when close to it as is the case at $\sqrt{s'} \sim 80$ GeV or $\sqrt{s'} \sim 113$ GeV [6]. In order to overcome this problem, the angular distribution is also binned in two regions defined by $\cos\theta \geq 0$ (forward hemisphere) and $\cos\theta < 0$ (backward hemisphere), which is equivalent to computing the forward-backward asymmetry without any hypothesis on the angular distribution.

In this case, the probability density for an event to be in the interval $x_i \leq x < x_{i+1}$ is given by

$$P(x, \cos\theta, s) \equiv \frac{1}{2\Delta x \sigma(s)} \int_{x_i}^{x_{i+1}} {\rm d}z H(s,z) \left(\sigma^0_{\rm T}(s(1-z)) + \epsilon(\theta) \sigma^0_{\rm FB}(s(1-z)) \right), \qquad (2)$$

where $\epsilon(\theta) = +1$ when $\cos\theta \geq 0$ and $\epsilon(\theta) = -1$ when $\cos\theta < 0$ and Δx is the bin size.

The simplest S-Matrix [2] parametrization for the process $e^+e^- \to \mu^+\mu^-$ predicts the total and the forward-backward cross sections to be

$$\sigma^0_{\rm T}(s) = \frac{4}{3}\pi\alpha^2 \left[\frac{g^{\rm tot}_\mu}{s} + \frac{s r^{\rm tot}_\mu + (s - \bar{M}^2_Z) j^{\rm tot}_\mu}{(s-\bar{M}^2_Z)^2 + \bar{M}^2_Z \bar{\Gamma}^2_Z} \right], \qquad (3)$$

$$\sigma^0_{\rm FB}(s) = \pi\alpha^2 \left[\frac{s r^{\rm fb}_\mu + (s - \bar{M}^2_Z) j^{\rm fb}_\mu}{(s-\bar{M}^2_Z)^2 + \bar{M}^2_Z \bar{\Gamma}^2_Z} \right]. \qquad (4)$$

Assuming that the photon exchange term $g^{\rm tot}_\mu$ is known from QED (as for the radiator function $H(s,x)$), the simplest S-matrix parametrization requires six parameters: $\bar{M}_Z, \bar{\Gamma}_Z, r^{\rm tot}_\mu, j^{\rm tot}_\mu, r^{\rm fb}_\mu$ and $j^{\rm fb}_\mu$.

The "r" parameters describe the measurements at the Z peak (dominated by the Z-exchange diagram in the SM), while the "j" parameters describe the energy dependence of the total and the forward-backward cross section, (dominated by the γ-Z interference in the SM). The parameters $\bar{M}_Z$ and $\bar{\Gamma}_Z$ are simply related to the usual definitions of the Z mass and width [2]:

$$\begin{aligned} \bar{M}_Z &= \frac{M_Z}{\sqrt{(1+\Gamma_Z^2/M_Z^2)}} \\ \bar{\Gamma}_Z &= \frac{\Gamma_Z}{\sqrt{(1+\Gamma_Z^2/M_Z^2)}} \end{aligned} \tag{5}$$

giving a shift in M_Z of 34 MeV and in Γ_Z of 0.9 MeV.

3 The ALEPH detector and event simulation

The ALEPH detector and its performance are described in detail elsewhere [7]. The features relevant to this analysis are briefly mentioned here.

The momentum of charged particles is reconstructed using the information given by the three tracking devices immersed in a 1.5 T axial magnetic field: a double-sided two-layer silicon vertex detector (VDET), an eight-layer axial-wire chamber (ITC) and a large time projection chamber (TPC), the last providing up to 21 space points for tracks of charged particles. An inverse transverse momentum resolution of 6×10^{-4} $(\mathrm{GeV})^{-1}$ is achieved (for 45 GeV muons) in the combined fit, while the resolution on $\cos\theta$ is better than 3×10^{-4} with a negligible impact on the analysis presented here.

The highly granular electromagnetic calorimeter (ECAL), located inside the magnetic coil, is made of 45 layers of lead and proportional wire chambers of a total thickness of 22 radiation lengths. ECAL is used to identify electrons and photons and measure their energy with a relative resolution of $0.18/\sqrt{E}$ (E in GeV).

Muons are identified by their characteristic penetration pattern in the hadron calorimeter (HCAL), a 1.2 m thick iron yoke instrumented with 23 layers of limited streamer tubes which provides a digital signal that gives a two-dimensional projection of the energy deposition, and a measurement of hadronic energy deposits. Muon identification is complemented with the measurement of three-dimensional hits in the two surrounding layers of muon chambers.

Photon candidates are identified by means of an algorithm [7] which performs a topological search for localized energy deposition in ECAL with a transverse and longitudinal profile consistent with that of an electromagnetic shower. The resolution achieved in the determination of the photon direction is better than 5 mrad.

In order to study the effect of the experimental cuts, more than 2×10^6 events were produced with full detector simulation, using the DYMU3 [8] and KORALZ 4.0 [9] Monte

Carlo generators for the exclusive and inclusive analysis, respectively, at several nominal LEP energies. Radiation of hard photons in the initial and final state is treated at $\mathcal{O}(\alpha)$ by DYMU3 and at $\mathcal{O}(\alpha^2)$ by KORALZ 4.0. In KORALZ the radiation of soft photons is included at all orders by exponentiation.

4 Event selection

As mentioned in the introduction, two different approaches have been followed. In both cases, the selection of dimuon events starts from the standard cuts applied in previous ALEPH [1] analyses, except that no cut on acollinearity or particle momentum is applied. This preselection completely rejects the hadronic background and most of the Bhabha events.

To reconstruct the effective centre-of-mass energy $\sqrt{s'}$, it is assumed that photons are emitted along the beam line, boosting the centre-of-mass system in that direction. In this approximation the magnitude of the boost β can be computed from the measured directions of the final state particles.

In the case of no FSR, the two charged particles are back to back in the centre-of-mass system of the incoming electron and positron after ISR. This condition determines β as a function of the measured polar angles of the two muon candidates (θ_1 and θ_2) through

$$| \beta | = \frac{| \sin(\theta_1 + \theta_2) |}{\sin\theta_1 + \sin\theta_2}. \tag{6}$$

If one also considers the possibility of having one radiated photon in the final state, the three particles ($\mu^+\mu^-\gamma_{\rm FS}$) will be contained in a plane in their centre-of-mass system. So, from the angles measured in the laboratory system (θ_i,ϕ_i) , one can compute β such that the relative angles in the centre-of-mass system θ'_{ij} satisfy the condition that defines a plane, $\theta'_{12} + \theta'_{23} + \theta'_{31} = 2\pi$.

Assuming the emission of only one ISR photon, s' can be determined from β. The energy radiated along the beam direction reads

$$E_\gamma^{\rm ISR} = \frac{| \beta |}{1+| \beta |}\sqrt{s}, \tag{7}$$

and, as a consequence, the fraction x of radiated beam energy can be expressed as:

$$x = \frac{2 | \beta |}{1+| \beta |}. \tag{8}$$

The only limitations come from the experimental resolution in the measurement of the directions of the detected particles and from the error induced by the ISR collinear approximation.

4.1 Selection of dimuon events with hard ISR

In the first analysis, an exclusive selection of dimuon events with hard ISR ($20 < \sqrt{s'} <$ 88 GeV), is performed. The effective centre-of-mass energy $\sqrt{s'}$ is computed with Eq. (6), i.e. assuming collinear ISR and no FSR.

Each muon candidate is required to have a momentum of at least 10 GeV and the sum of the momenta must be greater than 45 GeV. In order to eliminate the remaining background and dimuon events with FSR, the following cuts, C_i which are functions of the reconstructed $\sqrt{s'}$ and are given in table 1, are applied:

- $\sqrt{s'} - M_{\mu\mu} < C_1(\sqrt{s'})$, $M_{\mu\mu}$ being the invariant mass of the two muon candidates.
- $N_\gamma < 2$ and $|\cos\theta_\gamma| > C_2(\sqrt{s'})$.
- $| \phi_1 - \phi_2 - \pi | < C_3(\sqrt{s'})$, ϕ_i being the azimuthal angle of muon i.
- Missing $p_{\mathrm{T}} < C_4(\sqrt{s'})$.

The first cut removes both the $\tau\tau$ background and events with FSR. The efficiency of the selection procedure and the contamination by FSR are studied with a sample of simulated radiative muon events flagged as ISR or FSR on the basis of the generator information. This distinction is possible since no ISR-FSR interference is included at the generator (DYMU3) level. If initial, as well as final state photons are produced, the events are called ISR if the final state photon energy is below 1 GeV and FSR otherwise.

Data from the years 1992 to 1995 corresponding to a total integrated luminosity of 138 pb^{-1} at centre-of-mass energies in the range 89.4–93.0 GeV are used. A total of 986 di-muon events are selected compared to 1026.7 expected from Monte Carlo simulation, with 25 of the events coming from two photon background. The results of this direct comparison with the MC predictions are shown in table 2.

4.2 Inclusive selection

In this case, no specific selection of hard ISR events is made, and β is computed for all the identified dimuon candidates in the approximation that any detected photon is radiated in the final state. The only requirements added to the standard muon preselection are

- Only two charged tracks must be present with the momentum of the most energetic track being greater than 35 GeV.
- Only one photon candidate in ECAL with more than 0.3 GeV is allowed.
- The difference between the energy measured in ECAL and the corresponding energy computed from the event kinematics ($\sqrt{s}$, β and $\cos\theta$) must be less than four times the energy resolution in ECAL.

- The difference between $(\sqrt{s} - E_\gamma^{\rm ISR})$ and the total energy measured in ALEPH must be less than four times the energy resolution. Here $E_\gamma^{\rm ISR}$ denotes the energy computed with Eq. (7).

The first cut completely eliminates the two-photon background, while the second cut removes those events with double FSR. Photons from ISR emitted at large angles, and therefore detected in ECAL, are removed by the third cut, or by the second one if there is also FSR. The last cut requires the total energy to be conserved, and eliminates most of the remaining $\tau\tau$ background which is thus reduced to 0.01%. The only remaining background is mis-identified Bhabha events (0.09%). The total efficiency of the selection of dimuon candidates is $(80.34 \pm 0.05)\%$ at the Z peak. The resolution on x is shown in fig. 1, the rms of the differences between the reconstructed ($x_{\rm rec}$), and generated fraction of radiated energy ($x_{\rm gen}$), is around 0.01 to be compared with a bin size of 0.04.

The probability density given by Eq. (2) is corrected for the experimental efficiency as a function of $x_{\rm rec}$. The efficiency $\epsilon^i_{\rm F(B)}$ for the F(B) hemisphere in the interval $x_i \leq x < x_{i+1}$ is computed using the KORALZ MC simulation. These efficiency functions have been computed for all the different LEP nominal energies.

The data sample used in the inclusive analysis was recorded in the years 1990 to 1995 at centre-of-mass energies from 88.2 to 136.2 GeV, and corresponds to a total integrated luminosity of 143.5 pb^{-1}. A total of 130 178 events pass the selection cuts.

5 Results and systematic studies

The probability density of Eq. (2), corrected for the experimental efficiency at each energy point, is used to build a log-likelihood function defined as the sum of the logarithms of the single-event probabilities. These probabilities are convolved with a Gaussian probability density of the beam energy spread. The residual effect due to ISR-FSR interference on $\sigma^0_{\rm FB}$ is taken into account by means of an analytic expression that computes such corrections at $\mathcal{O}(\alpha)$ [5].

The probability density of Eq. (2) which is normalized w.r.t. the variables x and $\cos\theta$, needs to be weighted with the luminosity taken at each energy point and normalized again ($\hat{P}$). The total number of events is used to build a new constraint

$$\chi^2_1 = \frac{(\sum_{i=1,N_p}\ \mathcal{L}_i(\sigma(s_i) - \sigma^{\rm fit}(s_i)))^2}{(\Delta)^2}, \tag{9}$$

where the error in the denominator Δ takes into account the systematic and statistical uncertainties in the determination of the total cross section and luminosities at each nominal centre-of-mass energy ($\sqrt{s_i}$). A second constraint (χ^2_2) is given by the experimental measurements of M_Z and Γ_Z, as determined from the ALEPH measurements of the hadronic line shape. The final function to be minimized taking into account the

above constraints is

$$l \;=\; -2 \sum_{i=1,N_{\rm evt}} \ln \hat{P}(x_i, \cos\theta_i, s_i) + \chi^2_1 + \chi^2_2. \qquad (10)$$

The results obtained are shown in table 3 together with the SM predictions. A χ^2 can be computed from the Poisson probability to have seen $N_i^{\rm obs}$ events in the interval $\sqrt{s'_{i+1}} > \sqrt{s'} \geq \sqrt{s'_i}$ when the expected number is $N_i^{\rm fit}$. The χ^2/d.o.f. for the fit shown in table 3 is 193.7/187, corresponding to a confidence level of 35%. The results are in agreement with the SM, and the statistical precision of the measurements of $j_\mu^{\rm tot}$ and $j_\mu^{\rm fb}$ is improved by a factor 1.4 compared with the results obtained using the convolved cross sections of ref. [14]. A direct comparison with the predictions of the fit as a function of the $\sqrt{s'}$ interval is shown in table 4.

From the definitions

$$\begin{aligned} \sigma^0_{\rm F}(\langle\sqrt{s'}\rangle) &\equiv \sigma^{\rm fit}_{\rm F}(\langle\sqrt{s'}\rangle)\frac{N^{\rm obs}_{\rm F}}{N^{\rm fit}_{\rm F}} \\ \sigma^0_{\rm B}(\langle\sqrt{s'}\rangle) &\equiv \sigma^{\rm fit}_{\rm B}(\langle\sqrt{s'}\rangle)\frac{N^{\rm obs}_{\rm B}}{N^{\rm fit}_{\rm B}}, \end{aligned}$$

a measurement of the total cross section and forward-backward asymmetry is obtained over a wide range of energies, where the effect of the ISR has been deconvolved. The results are shown in tables 5 and 6 for the exclusive and inclusive analyses, respectively. In fig. 2 and fig. 3 one can compare also these measurements with previous measurements made at PEP [10], PETRA [11] and TRISTAN [12] at lower energies. The low energy data from these experiments are corrected to include the effect of the running of the fine structure constant α.

Different sources of possible systematic errors on the measured S-matrix parameters have been investigated and reported in table 7:

- The statistical uncertainty due to the finite number of MC events used to determine $\epsilon^i_{F(B)}$ has been propagated in the fit.
- The uncertainty associated with the calculation at $\mathcal{O}(\alpha)$ of the ISR-FSR interference corrections has been evaluated from the data by comparing the change on the asymmetry after a cut on the radiated energy with that predicted by the analytic calculation. A discrepancy of $\sim$60% is observed and propagated to the S-matrix parameters. A similar conclusion on the size of these discrepancies between data and the $\mathcal{O}(\alpha)$ ISR-FSR interference analytic calculation can be found in ref. [13].
- The limitations of the MC simulation to reproduce the angular distribution of hard FSR photons emitted at large angles ($\theta_{13} > 100^o$) with respect to the muon direction has been considered. The variation of the S-matrix parameters obtained by removing these events from the final sample has been quoted as a systematic error.

- The effect of the remaining Bhabha background has also been considered as a source of systematic uncertainty.

- The uncertainty on the beam energy spread (~ 1 MeV) has been propagated in the fit, and the effect is completely negligible.

6 Limits on extra Z bosons

Many attempts to unify the strong and electroweak interactions predict additional neutral heavy gauge bosons Z′. New interference terms, such as γ-Z′ and Z-Z′ would appear at the Born level and would modify the cross section and angular distribution at energies far from $\sqrt{s} \sim M_Z$.

After specifying the model (without any assumption on the structure of the Higgs sector), only two free parameters remain: i) the mixing angle θ_3 between Z and Z′, and ii) the mass of the heavier-mass eigenstate, $M_{Z'}$.

To obtain exclusion limits, a χ^2 is computed by comparing the values that appear in table 6 with different theoretical models. The ALEPH measurements of the hadronic cross section reported in [14] are also included, but they only improve the sensitivity to the mixing angle.

Four of the most popular models that introduce a new Z boson are considered. Three of them (χ, ψ and η models) are superstring-inspired models [15] based on the E_6 symmetry group. The other one is a left-right symmetric model [16] that includes a right-handed $SU(2)_R$ extension of the Standard Model gauge group $SU(2)_L \otimes U(1)$. These kind of models are characterized by the parameter $\alpha_{\mathrm{L-R}}$ that describes the coupling of the Z′ to fermions. The specific value $\alpha_{\mathrm{L-R}} = 1$ is chosen as typical example.

The effects of the Z′ for the L-R and E_6 models on the cross sections and asymmetries are calculated using an addition to the ZFITTER program, called ZEFIT (vers. 3.1) [17], that provides radiatively corrected cross sections and asymmetries for the process $e^+e^- \to f\bar{f}$. As the standard Z mass changes due to the presence of a mixed Z′, M_Z is also fitted (using the direct M_Z measurement constraint) along with the mixing angle θ_3 and the Z′ mass.

The region defined by $\chi^2 < \chi^2_{\mathrm{min}} + 5.99$ corresponds to a 95% confidence level one-sided exclusion bound on two parameters. This is plotted in fig. 4 for the models considered, and in table 8 the explicit limits are given. They are computed with $\alpha_s = 0.120 \pm 0.003$, $M_t = 175 \pm 6$ GeV and $M_H = 150^{+150}_{-90}$ GeV. In fig. 4 the exclusion limits published by CDF [18] in a direct search for Z′ bosons are also shown.

7 Conclusions

An exclusive selection of hard ISR events has been performed. A total of 986 events are selected, and good agreement with the Standard Model expectations is observed at centre-of-mass energies between 20 and 88 GeV.

Going one step further, the full statistical power of the event sample has been used by reconstructing the effective centre-of-mass energy $\sqrt{s'}$ on an event-by-event basis. A precise measurement of the total cross section and the forward-backward asymmetry in a range of energies still uncovered by present accelerators, extending from 60 to 136 GeV, has been performed. As a result, the S-matrix parameters that describe, in a general way, the energy dependence of these observables are determined with an unprecedented precision.

The results obtained for the S-matrix parameters are

$$\begin{aligned} r_\mu^{\rm tot} &= 0.14186 \pm 0.00080 \pm 0.00004 \\ j_\mu^{\rm tot} &= -0.033 \pm 0.022 \pm 0.007 \\ r_\mu^{\rm fb} &= 0.00273 \pm 0.00054 \pm 0.00032 \\ j_\mu^{\rm fb} &= 0.807 \pm 0.026 \pm 0.013, \end{aligned}$$

where the second error corresponds to the systematic uncertainty in the extraction of these parameters.

The improved precision on the measured energy dependence, especially the energy dependence of the forward-backward asymmetry $j_\mu^{\rm fb}$, allows the existing limits from LEP on $M_{Z'}$ to be improved.

Acknowledgments

It is a pleasure to thank our colleagues in the accelerator division of CERN for the excellent performance of the LEP accelerator. Thanks are also due to the technical personnel of the collaborating institutions for their support in constructing and maintaining the ALEPH experiment. Those of us not from member states wish to thank CERN for its hospitality.

References

[1] ALEPH Coll., D. Buskulic *et al.*, Z. Phys. **C62** (1994) 539;
DELPHI Coll., P. Abreu *et al.*, Nucl. Phys. **B418** (1994) 403;
L3 Coll., M. Acciarri *et al.*, Z. Phys. **C62** (1994) 551;
OPAL Coll., R. Akers *et al.*, Z. Phys. **C61** (1994) 19.

[2] R.G. Stuart, Phys. Lett. **B272** (1991) 353;
A. Leike, T. Riemann and J. Rose, Phys. Lett. **B273** (1991) 513;
T. Riemann, Phys. Lett. **B293** (1992) 451.

[3] OPAL Coll., P.D. Acton *et al.*, Phys. Lett. **B273** (1991) 338;
DELPHI Coll., P. Abreu *et al.*, Z. Phys. **C65** (1995) 603;
L3 Coll., M. Acciarri *et al.*, Phys. Lett. **B374** (1996) 331.

[4] F.A. Berends, G.J.H. Burgers and W.L. Van Neerven, Phys. Lett. **B185** (1987) 395;
Nucl. Phys. **B297** (1988) 429 and Nucl. Phys. **B304** (1988) 921 (E).

[5] D. Bardin *et al.*, Nucl. Phys. **B351** 1 (1991).

[6] J.-M. Frere, V.A. Novikov and M.I. Vysotsky, *Zeroes of the* $e^+e^- \to \bar{f}f$ *cross section and search for new physics*, ULB-TH/96-5, hep-ph/9605241.

[7] ALEPH Coll., D. Decamp *et al.*, Nucl. Instrum. and Methods **A294** (1990) 121 and **A360** (1995) 481.

[8] J.E. Campagne and R. Zitoun, Z. Phys. **C43** (1989) 469; and Proc. of the Brighton Workshop on Radiative Corrections, Sussex, July 1989. Proceedings by N. Dombey and F. Boudjema (eds.).

[9] S. Jadach, B.F.L. Ward and Z. Was, Comp. Phys. Comm. **79** (1994) 503.

[10] HRS Coll., M. Derrick *et al.*, Phys. Rev. **D31** (1985) 2352;
MAC Coll., W. W. Ash *et al.*, Phys. Rev. Lett. **55** (1985) 1831;
MARK II Coll., M. E. Levi *et al.*, Phys. Rev. Lett. **51** (1983) 1941.

[11] CELLO Coll., H. J. Behrend *et al.*, Phys. Lett. **B191** (1987) 209;
JADE Coll., W. Bartel *et al.*, Z. Phys. **C26** (1985) 507;
MARK J Coll., B. Adeva *et al.*, Phys. Rev. **D38** (1988) 2665;
PLUTO Coll., Ch. Berger *et al.*, Z. Phys. **C21** (1983) 53;
TASSO Coll., W. Braunschweig *et al.*, Z. Phys. **C40** (1988) 163.

[12] AMY Coll., C. Velissaris *et al.*, Phys. Lett. **B331** (1994) 227;
TOPAZ Coll., B. Howell *et al.*, Phys. Lett. **B291** (1992) 206;
VENUS Coll., K. Abe *et al.*, Z. Phys. **C48** (1990) 13.

[13] DELPHI Coll., P. Abreu et al., *First Study of the Interference between Initial and Final State Radiation at the Z resonance.* CERN-PPE/96-44 (March 1996), submitted to Z. Phys.

[14] ALEPH Coll., *Preliminary results on Z production cross sections and lepton forward-backward asymmetries using 1995 data.* Paper contributed to XXVIII International Conference on High Energy Physics, ICHEP'96, Warsaw, Poland, July 1996 PA07-069, and references therein.

[15] P.Langacker, R.W.Robinett and J.L.Rosner, Phys. Rev. **D30** (1984) 1470;
D.London and J.L.Rosner, Phys. Rev. **D34** (1986) 1530.

[16] J.C.Pati and A.Salam, Phys. Rev. **D10** (1974) 275;
R.N.Mohapatra and J.C.Pati, Phys. Rev. **D11** (1975) 566.

[17] A. Leike, S. Riemann and T. Riemann, Munich University Preprint LMU-91/06, and FORTRAN program ZEFIT;
A. Leike, S. Riemann and T. Riemann, Phys. Lett. **B291** (1992) 187.

[18] CDF Coll., F. Abe *et al.*, Phys. Rev. **D51** (1995) 949.

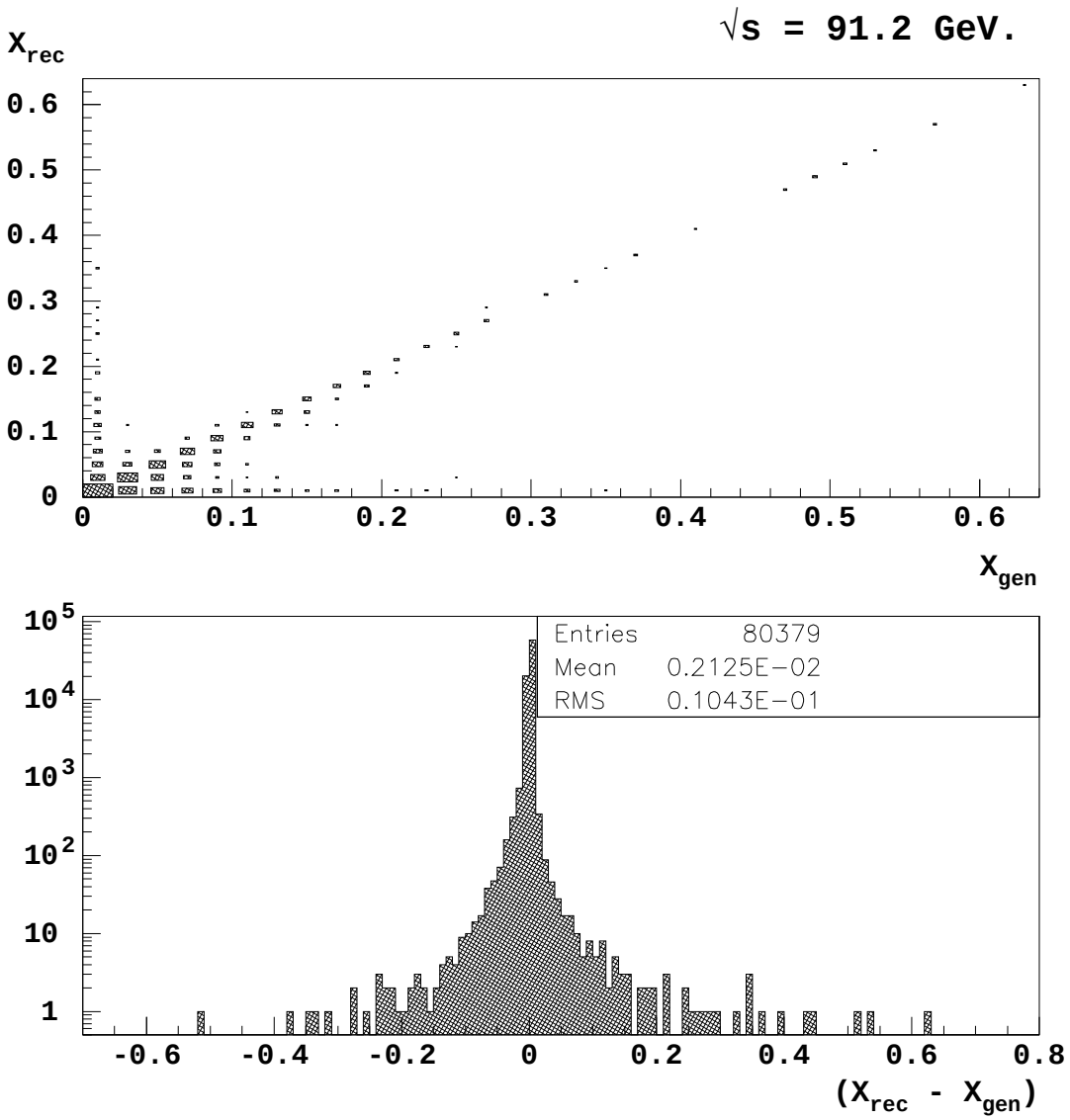

Figure 1: Monte Carlo study of the performance of the $s' \equiv s(1-x)$ reconstruction at $\sqrt{s} = 91.2$ GeV. The upper figure shows the correlation between the reconstructed $x_{\rm rec}$, and the generated $x_{\rm gen}$ values of x. The size of the squares is proportional to the logarithm of the number of events. The lower figure shows the distribution of the difference $x_{\rm rec} - x_{\rm gen}$.

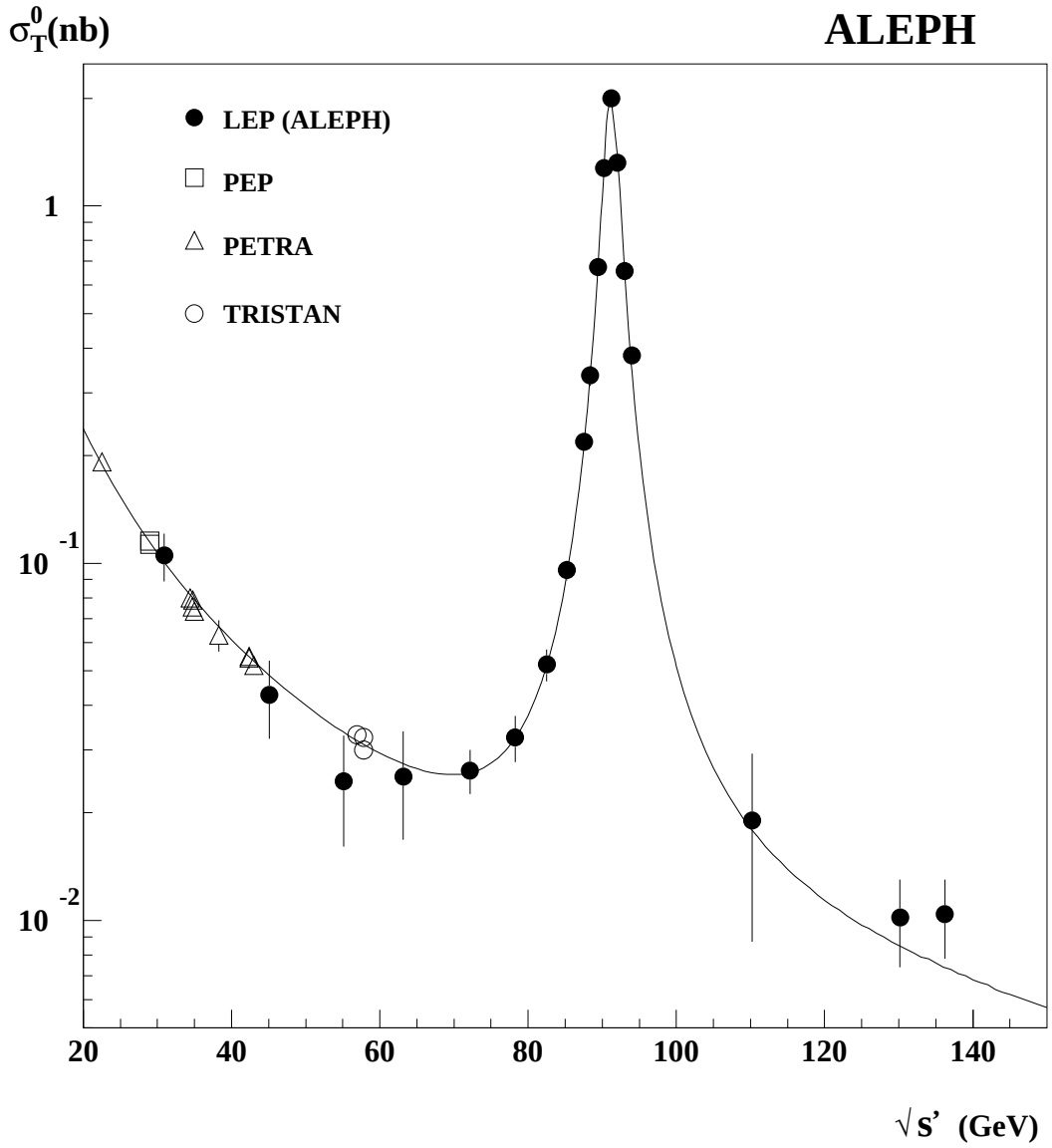

Figure 2: Measured cross sections of muon-pair production compared with the fit results. The ALEPH measurements below 60 GeV correspond to the exclusive hard ISR selection that are not used in the fit. For comparison the measurements at lower energies from PEP, PETRA and TRISTAN are included.

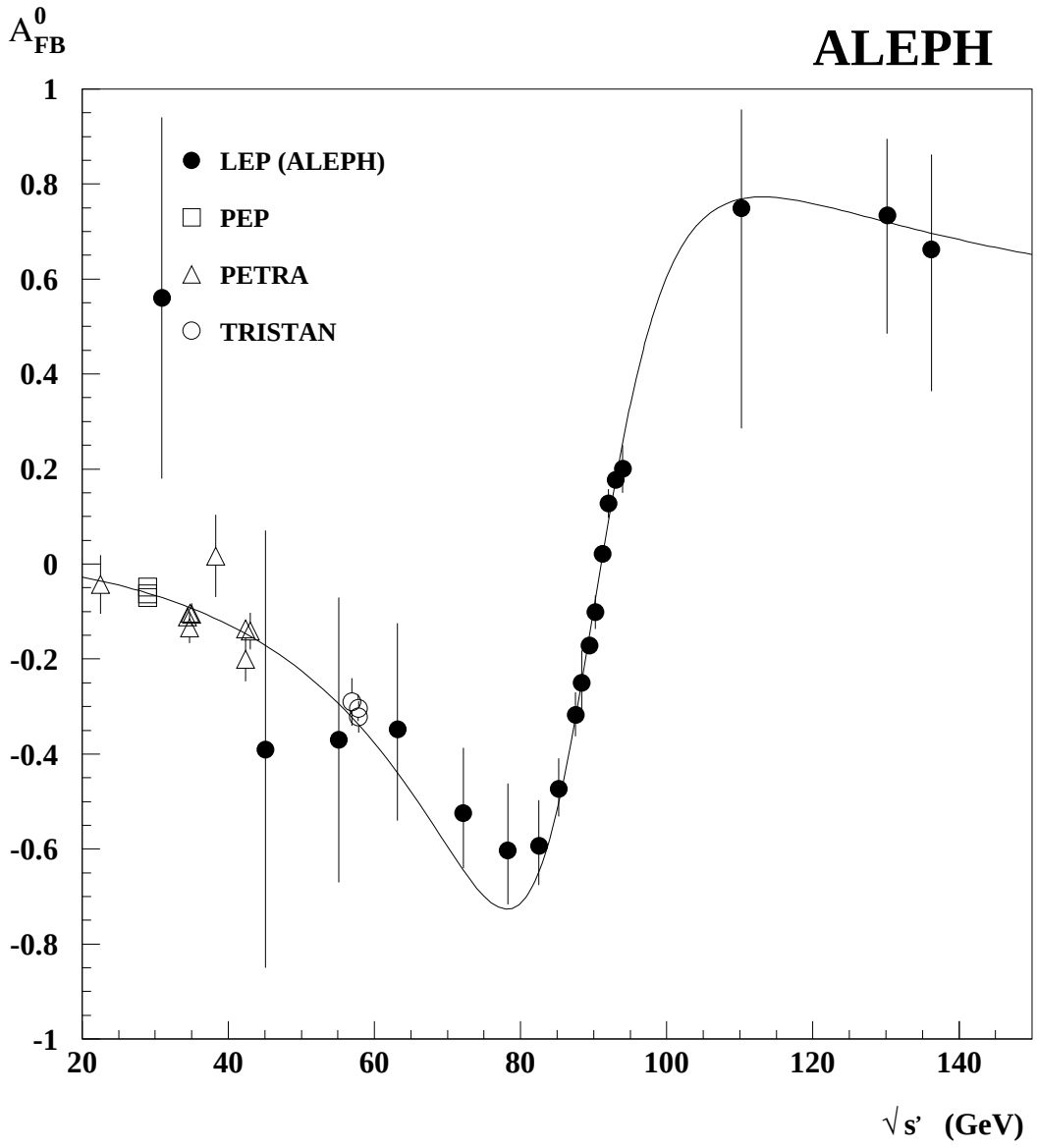

Figure 3: Measured forward-backward asymmetries of muon-pair production compared with the fit results. The ALEPH measurements below 60 GeV correspond to the exclusive hard ISR selection that are not used in the fit. For comparison the measurements at lower energies from PEP, PETRA and TRISTAN are included.

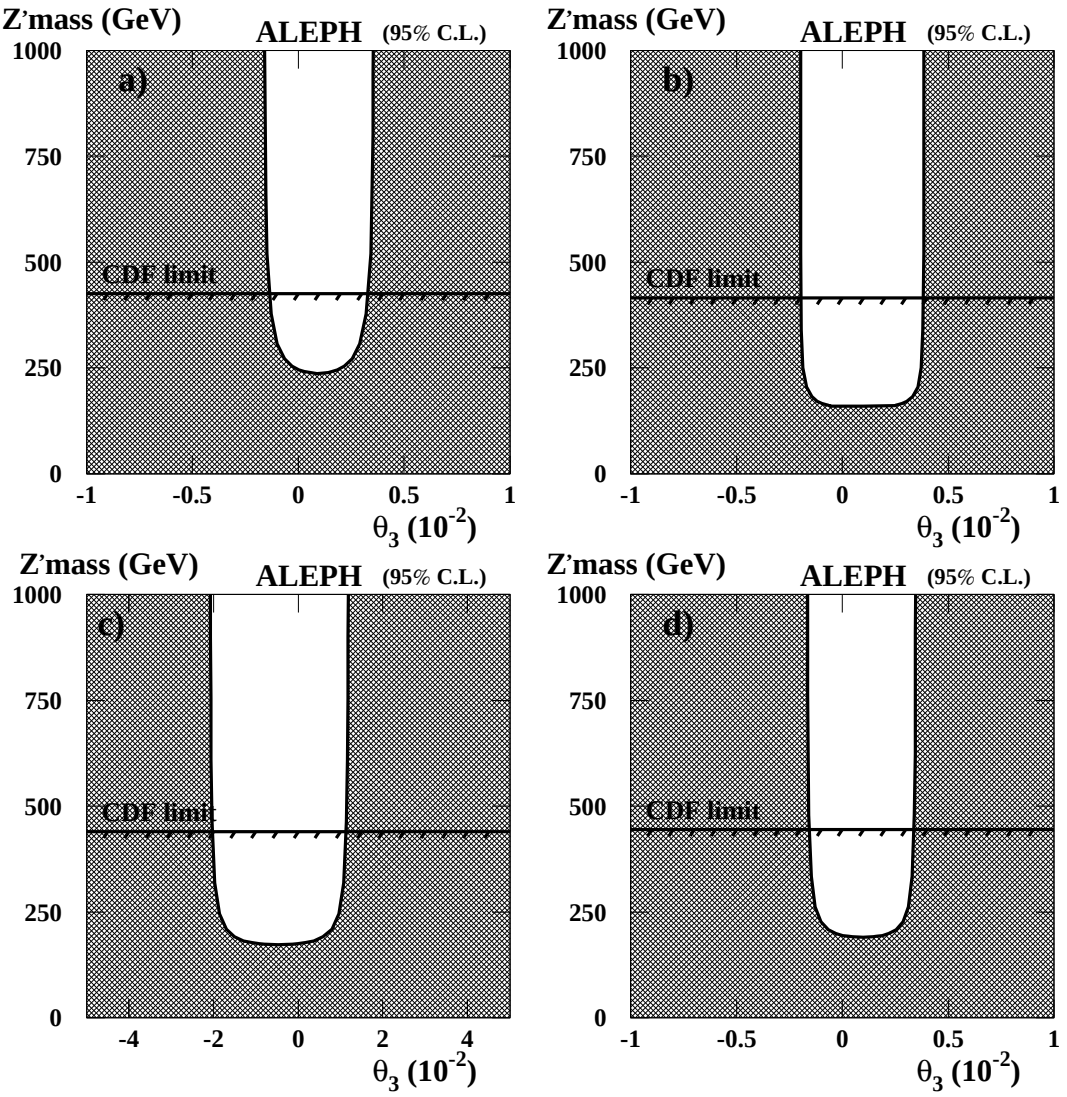

Figure 4: Curves corresponding to 95% confidence level contours dividing the $M_{Z'}$ - θ_3 plane into allowed and excluded (shaded) regions. a) χ model, b) ψ model, c) η model and d) Left-Right model with $\alpha_{\mathrm{L-R}} = 1$.

Tables

Table 1: Cuts used to identify hard ISR events as a function of the reconstructed effective centre-of-mass energy.

$\sqrt{s'}$ (GeV)	C_1 (GeV)	C_2	C_3 (rads)	C_4 (GeV)
$20-30$	20	0.60	1.0	10
$30-40$	15	0.60	0.2	8
$40-50$	10	0.94	0.2	6
$50-60$	8	0.94	0.1	5
$60-70$	6	0.94	0.05	5
$70-80$	3	0.94	0.03	5
$80-85$	2	0.94	0.02	5
$85-87$	2	0.94	0.02	5
$87-88$	2	0.94	0.02	5

Table 2: Number of observed hard ISR events in the different intervals of $\sqrt{s'}$ compared with the number of events predicted by the Monte Carlo and the expected number of two-photon background events. The pull is defined to be $(N^{\rm obs}-N^{\rm MC})/(\delta N)$. The efficiency and purity of the selection w.r.t. FSR events are shown in the last two columns.

$\sqrt{s'}$ (GeV)	$\langle\sqrt{s'}\rangle$ (GeV)	$N^{\rm obs}$	$N^{\rm MC}$	Pull	$N_{\gamma\gamma}$ Backg.	Efficiency	Purity
$20-40$	30.94	56	54.5	$+0.2$	14.3	0.81	0.95
$40-50$	45.11	28	31.0	-0.5	9.0	0.71	0.93
$50-60$	55.12	17	23.8	-1.3	0.0	0.69	0.96
$60-70$	65.15	33	36.1	-0.5	1.8	0.67	0.92
$70-80$	76.08	77	74.9	$+0.2$	0.0	0.65	0.89
$80-85$	83.37	167	167.3	0.0	0.0	0.65	0.88
$85-87$	86.13	256	264.8	-0.5	0.0	0.71	0.91
$87-88$	87.53	345	354.8	-0.5	0.0	0.74	0.92

Table 3: Results obtained for the S-matrix parameters from a maximum likelihood fit to the events selected in the inclusive analysis. The SM predictions are computed with $M_Z = 91.1863$ GeV, $\alpha^{-1}(M_Z^2) = 128.896$, $M_t = 175$ GeV and $M_H = 150$ GeV.

	SM predictions	Fit results	Correlation matrix			
$r_\mu^{\rm tot}$	0.14298	0.14186 ± 0.00080	1.00	0.04	0.04	0.11
$j_\mu^{\rm tot}$	0.004	-0.033 ± 0.022		1.00	-0.04	-0.34
$r_\mu^{\rm fb}$	0.00278	0.00273 ± 0.00054			1.00	0.13
$j_\mu^{\rm fb}$	0.800	0.807 ± 0.026				1.00

Table 4: Number of observed events in the different intervals of $\sqrt{s'}$ for the inclusive analysis compared with the number of events predicted from the fit results. The pull is defined to be $(N^{\rm obs} - N^{\rm fit})/(\delta N)$.

$\sqrt{s'}$ GeV	$\langle\sqrt{s'}\rangle$ GeV	$N_{\rm F}^{\rm obs}$	$N_{\rm F}^{\rm fit}$	Pull	$N_{\rm B}^{\rm obs}$	$N_{\rm B}^{\rm fit}$	Pull
$55-65$	63.13	11	10.5	$+0.1$	17	19.9	-0.5
$65-75$	72.18	22	16.9	$+1.1$	37	39.9	-0.5
$75-80$	78.29	17	12.3	$+1.2$	35	38.0	-0.5
$80-84$	82.50	26	23.2	$+0.6$	74	76.9	-0.3
$84-86$	85.20	70	64.9	$+0.6$	169	168.1	$+0.1$
$86.-87.8$	87.49	160	153.2	$+0.5$	306	297.5	$+0.5$
$87.8-88.6$	88.37	89	89.0	0.0	145	143.9	$+0.1$
$88.6-89.6$	89.42	3336	3399.4	-1.1	4683	4562.9	$+1.8$
$89.6-90.3$	90.21	376	378.7	-0.1	459	438.4	$+1.0$
$90.3-91.3$	91.22	55258	54873.5	$+1.6$	53974	53778.6	$+0.8$
$91.3-92.3$	92.05	619	609.8	$+0.4$	511	536.8	-1.1
$92.3-93.3$	92.99	5268	5216.3	$+0.7$	4036	3985.3	$+0.8$
$93.3-100$	93.96	239	228.0	$+0.7$	183	154.1	$+2.3$
$100-127$	110.25	7	6.1	$+0.2$	1	1.7	0.0
$127-133$	130.17	17	13.8	$+0.7$	3	2.4	$+0.2$
$133-136$	136.21	13	9.3	$+1.0$	3	1.8	$+0.6$

Table 5: Measured cross sections and asymmetries in the exclusive analysis compared with those predicted from the fit results. The pull is defined to be $(\sigma^0 - \sigma^{\rm fit})/(\delta\sigma^0)$ and $(A_{\rm FB}^0 - A_{\rm FB}^{\rm fit})/(\delta A_{\rm FB}^0)$.

$\langle\sqrt{s'}\rangle$ (GeV)	$\sigma^0 \pm \delta\sigma^0$ (nb)	$\sigma^{\rm fit}$ (nb)	Pull	$A_{\rm FB}^0 \pm \delta A_{\rm FB}^0$	$A_{\rm FB}^{\rm fit}$	Pull
30.94	0.105 ± 0.016	0.1009	$+0.3$	$+0.56 \pm 0.38$	-0.07	$+1.7$
45.11	0.043 ± 0.011	0.0487	-0.6	-0.39 ± 0.46	-0.17	-0.5
55.12	0.0245 ± 0.0084	0.0339	-1.1	-0.37 ± 0.30	-0.29	-0.3
65.15	0.0243 ± 0.0057	0.0268	-0.5	-0.44 ± 0.28	-0.48	$+0.2$
76.08	0.0291 ± 0.0034	0.0292	0.0	-0.52 ± 0.14	-0.70	$+1.4$
83.37	0.0610 ± 0.0048	0.0612	0.0	-0.62 ± 0.08	-0.60	-0.1
86.13	0.1191 ± 0.0076	0.1241	-0.6	-0.28 ± 0.07	-0.43	$+2.2$
87.53	0.210 ± 0.011	0.2163	-0.5	-0.33 ± 0.06	-0.32	-0.1

Table 6: Measured cross sections and asymmetries in the inclusive analysis compared with those predicted from the fit results. The pull is defined to be $(\sigma^0 - \sigma^{\rm fit})/(\delta\sigma^0)$ and $(A^0_{\rm FB} - A^{\rm fit}_{\rm FB})/(\delta A^0_{\rm FB})$.

$\langle\sqrt{s'}\rangle$ (GeV)	$\sigma^0 \pm \delta\sigma^0$ (nb)	$\sigma^{\rm fit}$ (nb)	Pull	$A^0_{\rm FB} \pm \delta A^0_{\rm FB}$	$A^{\rm fit}_{\rm FB}$	Pull
63.12	0.0253 ± 0.0085	0.0278	-0.3	$-0.35^{+0.22}_{-0.19}$	-0.435	$+0.5$
72.18	0.0263 ± 0.0037	0.0263	0.0	$-0.52^{+0.14}_{-0.12}$	-0.637	$+1.0$
78.29	0.0325 ± 0.0048	0.0330	-0.1	$-0.60^{+0.14}_{-0.11}$	-0.716	$+1.0$
82.50	0.0520 ± 0.0053	0.0525	-0.1	$-0.593^{+0.096}_{-0.082}$	-0.641	$+0.6$
85.20	0.0956 ± 0.0061	0.0934	$+0.4$	$-0.472^{+0.063}_{-0.059}$	-0.499	$+0.5$
87.49	0.219 ± 0.010	0.2118	$+0.7$	$-0.317^{+0.047}_{-0.045}$	-0.324	$+0.1$
88.37	0.336 ± 0.022	0.3341	$+0.1$	-0.250 ± 0.067	-0.246	-0.1
89.42	0.6759 ± 0.0075	0.6710	$+0.6$	-0.171 ± 0.011	-0.149	-2.0
90.21	1.276 ± 0.044	1.2487	$+0.6$	-0.101 ± 0.036	-0.075	-0.7
91.23	2.0018 ± 0.0060	1.9911	$+1.8$	0.0216 ± 0.0030	0.0199	$+0.6$
92.05	1.322 ± 0.040	1.3403	-0.5	0.128 ± 0.030	0.096	$+1.0$
92.99	0.6570 ± 0.0068	0.6498	$+1.1$	0.178 ± 0.010	0.179	-0.1
94.03	0.381 ± 0.018	0.3466	$+1.9$	0.201 ± 0.049	0.260	-1.2
110.46	0.019 ± 0.010	0.0175	$+0.1$	$0.75^{+0.21}_{-0.46}$	0.788	-0.2
130.20	0.0102 ± 0.0028	0.0083	$+0.7$	$0.73^{+0.16}_{-0.25}$	0.736	0.0
136.21	0.0104 ± 0.0026	0.0072	$+1.2$	$0.66^{+0.20}_{-0.30}$	0.712	$+0.2$

Table 7: Contributions to the total systematic uncertainties on the S-matrix parameters.

Source	$\Delta r^{\rm tot}_\mu$	$\Delta j^{\rm tot}_\mu$	$\Delta r^{\rm fb}_\mu$	$\Delta j^{\rm fb}_\mu$
MC statistics	0.00003	0.006	0.00003	0.009
ISR-FSR interf.	0.00002	0.002	0.00032	0.009
FSR	nil	0.003	0.00005	0.004
background	nil	0.001	0.00002	0.003
TOTAL	0.00004	0.007	0.00032	0.013

Table 8: 95% confidence level limits on $M_{Z'}$ and θ_3 from fits to the predictions of several models.

	$E_6(\chi)$	$E_6(\psi)$	$E_6(\eta)$	L$-$R($\alpha_{LR} = 1$)
$M_{Z'}$ (GeV) $>$	236	160	173	190
θ_3 (rads) $>$	-0.0016	-0.0020	-0.021	-0.0017
θ_3 (rads) $<$	$+0.0036$	$+0.0038$	$+0.012$	$+0.0035$